

Brief Report

Feasibility of Wave Intensity Analysis from 4D Cardiovascular Magnetic Resonance Imaging Data

Froso Sophocleous ^{1,†}, Kiril Delchev ^{1,2,†}, Estefania De Garate ^{1,2} , Mark C. K. Hamilton ², Massimo Caputo ^{1,2}, Chiara Bucciarelli-Ducci ^{1,3,4} and Giovanni Biglino ^{1,5,*} ¹ Bristol Heart Institute, Bristol Medical School, University of Bristol, Bristol BS8 1QU, UK² University Hospitals Bristol and Weston NHS Foundation Trust, Bristol BS1 3NU, UK³ Royal Brompton and Harefield Hospitals, Guys and St Thomas NHS Trust, London UB9 6JH, UK⁴ School of Biomedical Engineering and Imaging Sciences, Faculty of Life Sciences and Medicine, Kings College London, London WC2R 2LS, UK⁵ National Heart and Lung Institute, Imperial College London, London SW7 2BX, UK

* Correspondence: g.biglino@bristol.ac.uk; Tel.: +44-117-342-3287

† These authors contributed equally to this work.

Abstract: Congenital heart defects (CHD) introduce haemodynamic changes; e.g., bicuspid aortic valve (BAV) presents a turbulent helical flow, which activates aortic pathological processes. Flow quantification is crucial for diagnostics and to plan corrective strategies. Multiple imaging modalities exist, with phase contrast magnetic resonance imaging (PC-MRI) being the current gold standard; however, multiple predetermined site measurements may be required, while 4D MRI allows for measurements of area (A) and velocity (U) in all spatial dimensions, acquiring a single volume and enabling a retrospective analysis at multiple locations. We assessed the feasibility of gathering hemodynamic insight into aortic hemodynamics by means of wave intensity analysis (WIA) derived from 4D MRI. Data were collected in $n = 12$ BAV patients and $n = 7$ healthy controls. Following data acquisition, WIA was successfully derived at three planes (ascending, thoracic and descending aorta) in all cases. The values of wave speed were physiological and, while the small sample limited any clinical interpretation of the results, the study shows the possibility of studying wave travel and wave reflection based on 4D MRI. Below, we demonstrate for the first time the feasibility of deriving wave intensity analysis from 4D flow data and open the door to research applications in different cardiovascular scenarios.

Keywords: aorta; bicuspid aortic valve; magnetic resonance imaging; aortic valve; wave intensity analysis; hemodynamics; aortic distensibility; wave reflection; arterial waves



Citation: Sophocleous, F.; Delchev, K.; De Garate, E.; Hamilton, M.C.K.; Caputo, M.; Bucciarelli-Ducci, C.; Biglino, G. Feasibility of Wave Intensity Analysis from 4D Cardiovascular Magnetic Resonance Imaging Data. *Bioengineering* **2023**, *10*, 662. <https://doi.org/10.3390/bioengineering10060662>

Academic Editors: Hwa Liang Leo and Hamed Keramati

Received: 1 March 2023

Revised: 26 April 2023

Accepted: 3 May 2023

Published: 31 May 2023



Copyright: © 2023 by the authors. Licensee MDPI, Basel, Switzerland. This article is an open access article distributed under the terms and conditions of the Creative Commons Attribution (CC BY) license (<https://creativecommons.org/licenses/by/4.0/>).

1. Introduction

An estimated 1.35 million babies are diagnosed each year globally with congenital heart disease (CHD) [1]. The presence of different defects affects blood flow. Haemodynamic changes are observed, for example, in patients with valvular conditions such as bicuspid aortic valve (BAV), with deranged aortic blood flow characterised by a helical pattern [2]. This exposes the aortic valve and ascending aorta to abnormal stress, which is considered one of the drivers of aortopathy in these patients [3]. Hence, flow assessment and quantification in patients with CHD can not only provide pathophysiological insights but also potentially inform treatment. Cross-sectional imaging is an invaluable tool to perform such hemodynamic assessment [4,5]. Cardiac magnetic resonance imaging (MRI), in particular, is a non-invasive, non-ionising and sensitive tool for both the diagnosis and follow-up of CHD patients, allowing for both anatomical and functional evaluation with high reproducibility and the ability of characterising tissues with different sequences [6]. In CHD, flow measurements are required at multiple sites [7]. The development of 4D MRI has allowed time-resolved 3D velocity phase-contrast (PC) imaging for evaluating

flows through the heart valves, vascular structures and heart chambers [8]; measuring velocity (U) data throughout the cardiac cycle in all three spatial directions; and enabling the visualization of multidirectional flow patterns [9]. Furthermore, the acquisition of a single volume allows the user flexibility for the retrospective placement of analysis planes at any point within that volume [10]. Measurements from 4D MRI have been validated, compared to 2D-PC MRI, as the primary method for the routine clinical quantification of aortic blood flow [11], overall showing good agreement in CHD [12–18]. Given the complex flow patterns typical of CHD [16,19], 4D MRI is emerging as a particularly appealing tool for hemodynamic assessment in CHD. In light of the opportunity of extracting U and vessel area (A) data at multiple locations along a volume, this also represents an opportunity to derive additional hemodynamic information at the post-processing stage by means of performing wave intensity analysis. This method allows for the assessment of the working condition of the heart in relation to the remainder of the vasculature (i.e., the ventriculo-arterial coupling). Wave intensity was introduced over 30 years ago for visualising and quantifying arterial waves [20]. Wave intensity, traditionally defined as the product of pressure and velocity differentials over a time interval [21], can also be derived from PC-MRI [22] and has been applied to CHD scenarios, providing valuable hemodynamic insights. Here, we wanted to assess the feasibility of performing the analysis from 4D MRI data, thus potentially extending its applicability and representing a promising tool for future studies on arterial wave dynamics.

2. Materials and Methods

2.1. Study Participants

Patients scheduled for aortic replacement (e.g., elephant trunk/whole arch replacement, Ross procedure and Ozaki procedure) were prospectively identified based on their BAV morphology and invited for an MRI scan. Healthy individuals without any known cardiovascular disease were recruited as controls. A total of $n = 12$ BAV patients and $n = 7$ volunteers were recruited for the study. Exclusion criteria included patients with previous aortic valve replacement (AVR) or other aortic interventions, patients with connective tissue disorders or syndromes, patients with metal body implants or permanent metal fragments, pregnancy, claustrophobia and severe kidney dysfunction (i.e., estimated glomerular filtration rate < 60 mL/min/1.73 m²) [23]. Demographic and clinical data were obtained from the patients' hospital records, including valve phenotype (i.e., right-left (RL), right-non-coronary (RNC) and left-non-coronary (LCN) fusion), degree of aortic stenosis (AS) and regurgitation (AR), type of dilation (one sided/overall) and presence of calcification. Imaging acquisition received Health Research Authority approval after being reviewed by the Research Ethics Committee (REC) (REC reference: 17/NI/0147).

2.2. Image Acquisition and Segmentation

The MRI scans were acquired at 3T (Magnetom, Skyra, Siemens Healthineers, Erlangen, Germany). An aortic 4D flow sequence was included for haemodynamic assessment. Sequence settings were as follows: velocity encoding (VENC): 150–400; temporal resolution (TR): 38.36 ms; echo time (TE): 2.1 ms. The acquisition time was 10–12 min.

Segmentation was performed with commercial software (CVI42 Flow package, Circle Cardiovascular Imaging, Calgary, Canada), which has been previously used for analysis of 4D flow data [24–27]. The appropriate volume (“mask”) was selected to encapsulate the whole aorta based on its anatomical markers. The aortic centreline was set automatically by the software and a manual threshold for the aortic volumes was set so that it would best fit the centreline at the highest flow through the vessel in systole. Upon reconstruction, the software requires position one or multiple planes perpendicular to the centreline along the vessel to perform analysis, including calculation of A and U waveforms at each plane. Three planes along the aorta were chosen for analysis: (1) in the ascending aorta above the sinotubular junction; (2) in the thoracic aorta just after the brachiocephalic vessels; (3) in the descending aorta above the diaphragm. Position 1 was chosen due to the anatomical

(hence, haemodynamic) variability typical of BAV patients. Position 2 was selected as the brachiocephalic bifurcations in the aortic arch, which represents the first major (lumped) reflection site along the aorta. Position 3 was selected in order to establish any further changes as the waves travel into the descending aorta.

Flow streamlines, flow displacement in the aorta and flow rate were measured. To allow precise delineation of the aortic wall, the operator was allowed to alter regions of interest (ROI) at each plane, and careful vessel segmentation for each frame was performed manually. The adjusted ROI was then used to calculate A and pinpoint the location in the phase image, which was used to calculate the U signal. The extracted A and U signals were then used to calculate wave intensity, as briefly explained in the next paragraph.

2.3. Wave Intensity Analysis

The A and U signals were processed with an in-house script (Matlab, MathWorks, Natick, MA, USA). The extracted values were smoothed using a Savitsky–Golay filter (window size: 5–11), due to the heterogeneity of the 4D data, and a second-degree polynomial. Separation of forward and backward wave components requires the measurement of wave speed c [21,22]. The Bramwell–Hill equation relates c to arterial distensibility [21], where ρ is blood density, and D is distensibility, which equals relative area change (dA/A) divided by pressure change (dP):

$$c^2 = \frac{1}{\rho D} = \frac{AdP}{\rho dA} \quad (1)$$

The water hammer equation also shows how c relates to dP and U change (dU), where the “+” subscript indicates forward waves and the “−” indicates backward ones:

$$dP_{\pm} = \pm \rho c dU_{\pm} \quad (2)$$

c using non-invasive parameters (i.e., replacing dP in Equation (1) with Equation (2)) can be expressed by the following equation:

$$c = \frac{AdU}{dA} = \frac{dU}{d \ln A} \quad (3)$$

This can also be arranged to express the water hammer in terms of U and A:

$$dU_{\pm} = \pm c d \ln A_{\pm} \quad (4)$$

Similarly to the PU loop method [28], U and $\ln A$ data were thus plotted to produce a U- $\ln A$ loop (Figure 1). The early systolic linear part of the loop yields c [29].

Considering arterial waves as a product of the summation of incremental wave fronts [21], U and A curves can be separated into their forward and backward constituents:

$$dU = dU_{+} + dU_{-} \quad (5)$$

$$d \ln A = d \ln A_{+} + d \ln A_{-} \quad (6)$$

These can be rearranged to obtain the following equations:

$$dU_{\pm} = \frac{1}{2}(dU \pm c d \ln A) \quad (7)$$

$$d \ln A_{\pm} = \frac{1}{2} \left(d \ln A \pm \frac{1}{c} dU \right) \quad (8)$$

The separated area-based intensity dI_A can be derived as product of dU_{\pm} and $dlnA_{\pm}$ above, whereas net dI_A is directly calculated as the product of the U and lnA differentials:

$$dI_A = dUdlnA \quad (9)$$

The resulting wave intensity pattern was analysed, at each plane, extracting peaks (i.e., intensity) and areas (i.e., energy) of the three typical dominant waves in systole, which include a forward compression wave (FCW) as a surrogate of left ventricular contractility, a forward expansion wave (FEW) as a surrogate of isovolumic relaxation and a backward compression wave (BCW) describing wave reflection. We refer the reader to the broader wave intensity literature for additional details on the methodology and clinical significance.

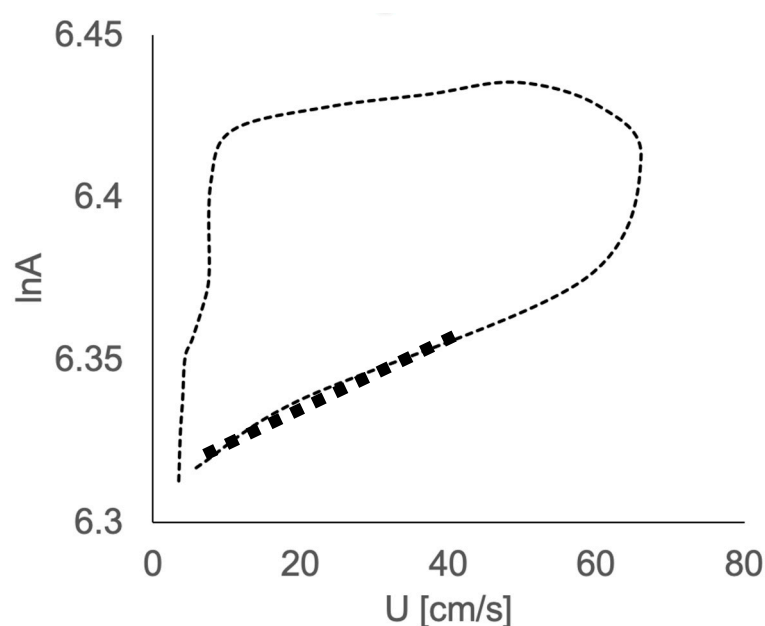


Figure 1. Example of velocity–area (U - lnA) loop, with the linear portion of the initial part of the loop yielding wave speed (in bold).

2.4. Statistical Analysis

The analysis was performed in Stata (v.13.1, StataCorp, College Station, TX, USA). Continuous data are reported as mean \pm standard deviation (SD) and categorical variables as percentages. The chi-square test was used to compare proportions. Differences between two continuous variables were tested with a Mann–Whitney test (e.g., BAV vs. control), and a Kruskal–Wallis test was performed to test continuous variables against independent ones, followed by a Dunn’s test post hoc (e.g., position 1 vs. position 2 vs. position 3). Univariate linear regression analysis was used to test for associations between clinical and anatomical variables as appropriate. Alpha level was set at $p < 0.05$.

3. Results

Out of the 19 participants who entered the study, 17 were eligible for analysis. One healthy volunteer and one BAV patient were excluded due to sub-optimal image quality. Patients ($n = 11$) were 54 ± 11 years old and 50% male with a BSA of 2.0 ± 0.2 m², while healthy volunteers ($n = 6$) were 41 ± 14 years old and 54% male with a BSA of 2.0 ± 0.07 m². Details about dilation type, valve phenotype, the degree of AS and/or AR and the presence of calcification were not available for one BAV patient; nonetheless these characteristics (which were not used for any analyses) are reported for completeness in Table 1.

Table 1. Baseline descriptive characteristics. BAV = bicuspid aortic valve; RL = right-left; RNC = right-non-coronary; LCN = left-non-coronary.

	Control (n = 6)	BAV (n = 10)
Ascending aorta dilatation type		
One-sided (n, %)	-	6 (60)
Overall (n, %)	-	4 (40)
Valve phenotype		
RL (n, %)	-	6 (60)
RNC (n, %)	-	3 (30)
LCN (n, %)	-	1 (10)
Degree of aortic regurgitation		
None (n, %)	-	4 (40)
Mild (n, %)	-	0
Moderate (n, %)	-	3 (30)
Severe (n, %)	-	3 (30)
Degree of aortic stenosis		
None (n, %)	-	3 (30)
Mild (n, %)	-	2 (20)
Moderate (n, %)	-	2 (20)
Severe (n, %)	-	3 (30)
Calcification present (n, %)	-	3 (30)

The aortas of all participants were successfully reconstructed (Figure 2). The visual assessment of the flow velocity and U streamlines of the two groups showed high U with turbulent helical flow in the BAV group and a lower, more laminar profile in the healthy volunteers, as expected. The successful extraction of U and A during the cardiac cycle for all participants was also performed from all three planes (the waveforms are shown in Figure 3).

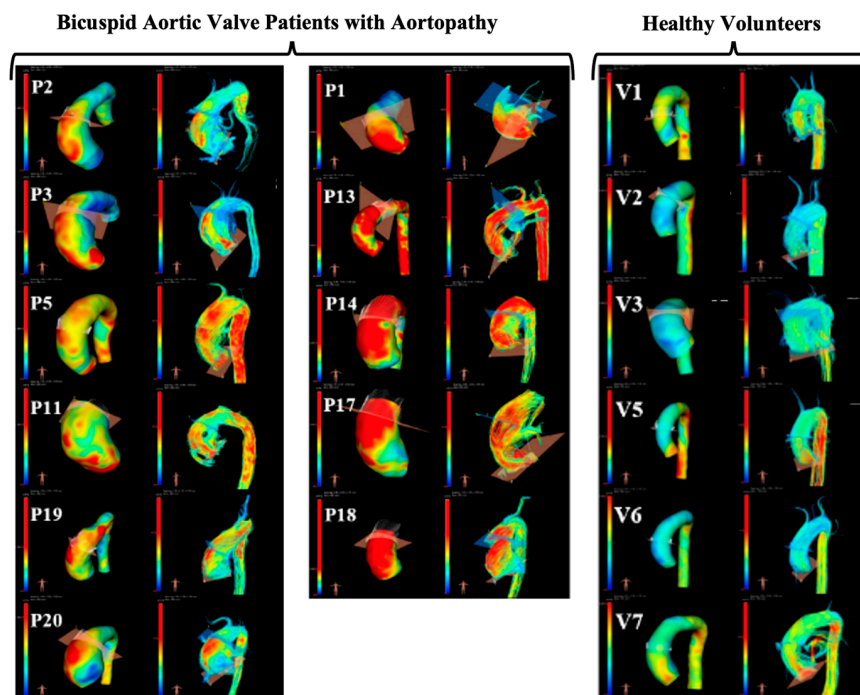


Figure 2. Illustration of 4D MRI analysis and qualitative comparison of wall shear stress maps and velocity streamlines (left and right in each pair of images, respectively). Patients (P) and volunteers (V) are all presented, and it is possible to qualitatively appreciate higher wall shear stress (yellow and red regions) and more helical flow in patients with bicuspid aortic valve, as expected.

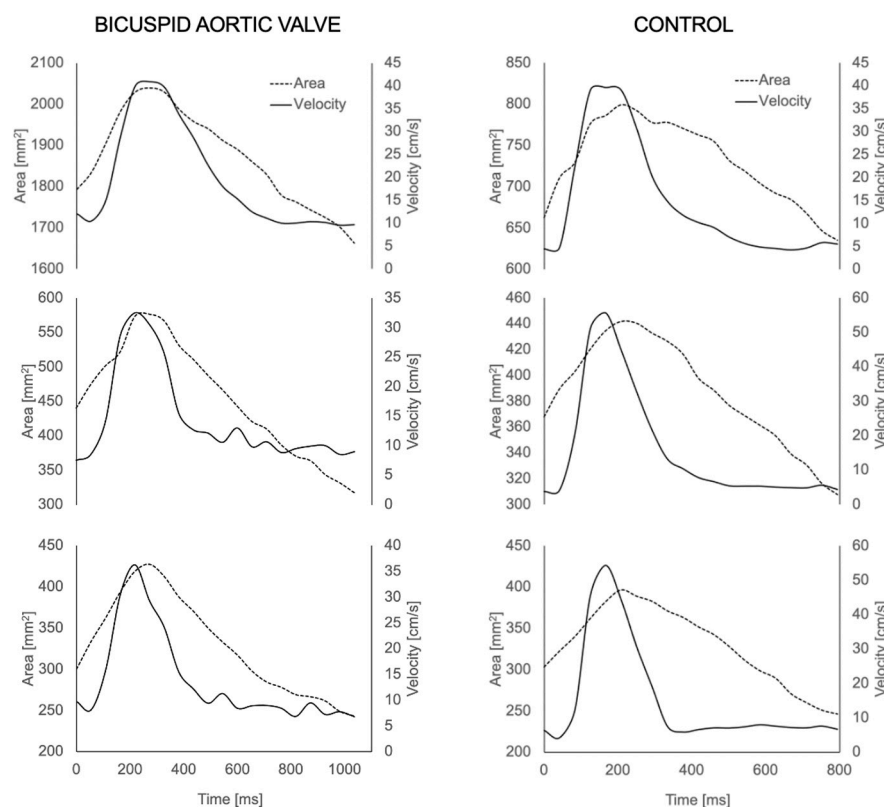


Figure 3. Area (A) and velocity (U) waveforms for each aortic plane (ascending, thoracic and descending aorta) extracted from the 4D MRI for a BAV patient (left) and healthy volunteer (right).

Examining the physiological data revealed a significantly higher mean U (U_{mean}) ($p = 0.004$), maximum systolic A (A_{max}) ($p = 0.0009$) and minimum diastolic A (A_{min}) ($p = 0.0009$) in the ascending aorta of the BAV population compared to the controls (Table 2).

Table 2. Summary of velocity (U) and area (A) data derived from 4D MRI.

	Ascending Aorta			Thoracic Aorta			Descending Aorta		
	Control	BAV	<i>p</i> Value	Control	BAV	<i>p</i> Value	Control	BAV	<i>p</i> Value
U_{peak} (cm/sec)	53.49 ± 14.5	58.42 ± 16.62	0.22	52.94 ± 17.60	58.40 ± 26.90	0.91	57.26 ± 21.5	48.35 ± 20.76	0.42
U_{mean} (cm/sec)	17.53 ± 3.73	33.74 ± 19.81	0.004	18.15 ± 1.83	32.16 ± 19.61	0.03	19.86 ± 3.54	26.92 ± 14.83	0.68
A_{max} (mm ²)	846.85 ± 197.2	1796.58 ± 353.82	0.0009	496.90 ± 197.27	739.044 ± 192.45	0.0049	411.43 ± 41.59	602.16 ± 173.73	0.0049
A_{min} (mm ²)	659.02 ± 115.82	1452.337 ± 303.52	0.0009	310.99 ± 17.13	437.43 ± 233.69	0.056	247.11 ± 34.47	322.94 ± 165.58	0.68

Overall, there was no significant difference in peak U between the planes in the BAV patients ($p = 0.19$) and the control population ($p = 0.67$). Similarly, no overall plane differences in mean U were seen in the BAV patients ($p = 0.15$) and the control group ($p = 0.36$).

The A_{max} during systole was significantly different across the three planes in the BAV group ($p = 0.0001$) and in the control group ($p = 0.0016$), and, similarly, the A_{min} during diastole was also significantly different across the three planes in the BAV group ($p = 0.0001$) and the control group ($p = 0.0005$).

An example of wave intensity signals generated in a BAV patient and a healthy volunteer are shown in Figure 4. Throughout all measurement sites, the control group exhibited higher c compared to the BAV group (Table 3). Overall, there was no significant difference in c between the planes in the BAV population ($p = 0.14$) and the healthy volunteers

($p = 0.34$). The only significant difference was observed within the BAV group, between the thoracic aorta and the descending aorta ($p = 0.03$). No significant relationship was observed between age and c in the ascending aorta ($R^2 = 0.20, p = 0.067$).

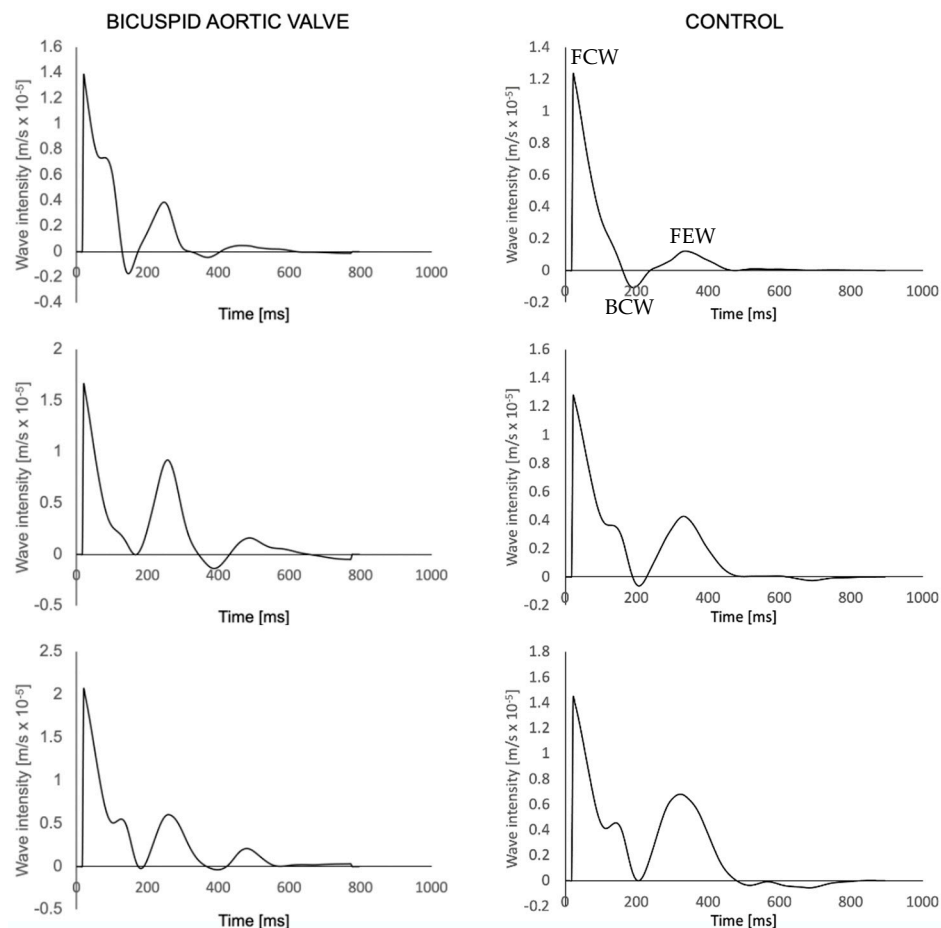


Figure 4. Wave intensity waveforms of a BAV patient (left) and a healthy volunteer (right) at the three aortic planes, sequentially from top to bottom. FCW = Forward compression wave; BCW = backwards compression wave; FEW = forward expansion wave (shown once to illustrate peaks).

Table 3. Summary of wave intensity analysis results including wave peaks (FCW = forward compression wave; FEW = forward expansion wave; BCW = backward compression wave).

	Ascending Aorta			Thoracic Aorta			Descending Aorta		
	Control	BAV	<i>p</i> Value	Control	BAV	<i>p</i> Value	Control	BAV	<i>p</i> Value
Wave speed $m\ s^{-1}$	6.40 ± 1.62	4.85 ± 1.75	0.09	5.90 ± 1.67	4.83 ± 1.44	0.19	5.11 ± 1.53	3.67 ± 1.77	0.04
FCW (m/s) $\times 10^{-5}$	1.01 ± 0.43	0.814 ± 0.58	0.22	1.18 ± 0.77	1.46 ± 0.81	0.36	1.62 ± 0.73	1.61 ± 0.64	0.48
BCW (m/s) $\times 10^{-5}$	-0.22 ± 0.20	-0.06 ± 0.07	0.10	-0.22 ± 0.23	-0.19 ± 0.36	0.48	-0.35 ± 0.33	-0.18 ± 0.34	0.08
FEW (m/s) $\times 10^{-5}$	0.08 ± 0.04	0.18 ± 0.11	0.07	0.27 ± 0.19	0.59 ± 0.58	0.22	0.47 ± 0.30	0.50 ± 0.55	0.54

4. Discussion

This study examined the feasibility of performing wave intensity analysis based on area and velocity data derived from 4D MRI scans in patients with BAVs and healthy volunteers, assessing the physiologically realistic nature of the results. The analysis could indeed be performed successfully in all cases, except in two in which images were deemed to be of sub-optimal quality for a 4D flow analysis. The results were physiologically meaningful, with mean U and A changes during systole and diastole significantly higher in the ascending and thoracic aorta of the BAV population compared to the control group (see

Table 2). No difference was observed in wave speed or any of the wave peaks. This study adds to the growing literature on wave intensity, demonstrating that the analysis can be performed using 4D MRI, hence allowing for the study of wave propagation over time in the same vessel during the same acquisition, which can be particularly insightful in CHD.

As illustrated in Figure 3, the U signals were realistic at all locations along the aorta, and a significantly higher mean U was observed in the ascending aorta of BAV patients. This is in line with previous literature findings in which U was also increased, which is largely due to the morphological nature of BAVs that leads to an eccentric flow jet [30–32]. This was also observed in the thoracic aorta. Although this comparison was not the main goal of the study and was limited by the sample size, the observation was intriguing, as flow abnormalities in BAVs have been reported to normalise at this point [33].

The observed significant difference in aortic area change is also physiologically sensible, as ascending aortic dilatation was present in 10 of the BAV patients (Table 1). As for the significantly higher A_{\max} in the thoracic aortas of the BAV patients, this could potentially indicate that the thoracic aorta is able to accommodate for the increased U and, thus, reflect a slightly increased distensibility.

The calculated c , at all three planes within our sample, fit well with previously published studies. These studies have focused both on various cardiovascular diseases [34] and healthy individuals with varying age [35,36] using PC-MRI, which is considered the gold standard for measuring blood flow in the aorta. Our c measurements are also supported by a study that focused solely on BAV patients and reported an average c of 4.2 m/s (range: 2.5–6.3 m/s) [37]. As reported in Table 3, c differences were not significant between the two groups within the ascending and thoracic aorta. In the context of BAVs, a decreased aortic distensibility compared to controls has been reported [38,39]. Our study did not find a significant difference in c in the ascending and thoracic segments, suggesting such a change in distensibility. Firstly, this could mean that the flow-induced tissue changes observed in BAV patients might not occur in conjunction with the global increase in aortic stiffness, at least not to the extent to which it can be captured with c quantification from 4D MRI [40]. Secondly, the presence of valvular conditions, such as AS or AR, can affect c measurements [41]. Additionally, one echocardiographic study, which used the aortic stiffness index, found no significant distensibility changes between BAV patients with AS and controls and suggested that the presence of AS could progressively reduce distensibility (and, hence, increase c) [42]. The varying degrees and presence of valvular disease in our group, combined with the small sample size, likely explain these results.

Interestingly, the control group exhibited a significantly higher c in the descending aorta ($p = 0.04$) than the BAV patients. Previous studies have shown that BAV populations present with higher c in the descending aorta even in the absence of concomitant valvular disease [43]. One study, however, did find that BAV patients had greater distensibility than those with tricuspid aortic valves [41]. The homogeneity of the valvular disease in our population, as mentioned above, could be a possible explanation. It is possible to speculate a more distensible or enlarged descending aorta in BAV patients, which has also been observed using computational modelling [44], making that segment more compliant, which would lead to lower c , as the A_{\max} in the BAV group was significantly higher compared to the controls (Table 2). This notion is also supported by the reduced aortic stiffness in patients with abdominal aortic aneurysms and the subsequent increase in stiffness after repair [45,46].

Numerous studies using different methodologies have concluded that c and, hence, stiffening increase linearly with age [47–49]. Our study did not find such a significant association ($p = 0.067$), which might be due to the small size of our population and its relatively youth (mean age 53.7 ± 11.4) compared to other studies, which had more varying age groups, some consisting of patients above the age of 66 [35]. Furthermore, there was no significant difference between the three main waves across groups, potentially suggesting that there is no major difference in VA coupling between the two groups. However, these observations should only be treated as preliminary and hypothesis-generating.

From a methodological standpoint, it is important to mention the temporal resolution at which the images were acquired. Lower temporal resolution is a known limitation of 4D MRI compared to the gold standard PC-MRI [8]. This could have affected c calculations as it is a parameter for which calculation requires high temporal resolution [22]. Future work in this context could experiment with higher temporal resolution 4D MRI.

From a clinical standpoint, the MRI scans used in this study were research and not clinical scans. While its value is increasingly recognised for clinical use, including in congenital heart disease and in aortic diseases [50], 4D flow is not routinely acquired as part of a cardiac MRI scan in many centres. A main limitation of 4D flow acquisition historically has been the long acquisition time, but techniques are increasingly being explored to reduce this and, thus, facilitate clinical implementation [51]. Nonetheless, demonstrating the feasibility of the technique opens the door to research applications and to the future exploration of clinical applications. Some examples of the clinical value of wave intensity include its potential to assess sub-clinical ventricular dysfunction [52] or to stratify hypertensive patients with different ventricular configurations [53]. The clinical relevance of wave intensity includes both mechanistic and prognostic insights, and it has been shown to be a highly sensitive measure in different scenarios, from aortic stenosis to left ventricular hypertrophy and heart failure [54]. Wave analysis has the potential to complement MRI-derived biomechanical and hemodynamic information with data on wave travel, wave reflection and ventriculo-arterial coupling.

5. Limitations

The study has several limitations. The first one is the small sample size, which inherently limited our ability to compare the BAV patients and the controls. Nevertheless, the aim of this work was to assess the feasibility of the proposed methodology to obtain realistic physiological data, which was achieved. This, in turn, would allow future research to generate appropriate hypotheses on wave parameters and analyse them accordingly, which will be interesting across several CHD scenarios.

The heterogeneity of the BAV population represented an additional limitation. The group had varying degrees and presences of valvular disease as well as different phenotypes of BAVs (Table 1). This could likely lead to an increase in the variability of the results as the different pathoanatomical features of BAVs can correspond to different unfavourable haemodynamic environments [55].

The segmentation method of this study is also a methodological point that warrants discussion as it still requires a significant amount of manual input. Although measuring A presents the advantage of not assuming vessel circularity [22], which can be particularly relevant in some CHD scenarios, e.g., after surgical repair, it is interesting to potentially move away from manual segmentation, strengthening the potential for future clinical applications of this methodology and similar ones. Current technological improvements have explored the use of machine learning to speed up the acquisition, flow measurement and—importantly—the analysis process with MRI data [56]. This would be particularly useful if the discussed methodology is applied to large cohorts of patients as 4D MRI datasets are inherently of a large volume [56].

Future work should apply the methodology to larger samples of patients and volunteers. This would not only improve the robustness of the results but also allow more in-depth analyses that explore variables including the BAV morphology and the additional assessment of haemodynamic parameters to compare against the wave intensity data. Increasing the temporal resolution would allow the easier manual handling of the segmentation as well as more reliable calculations of c .

6. Conclusions

This work demonstrates that it is feasible to derive wave intensity analysis from 4D MRI in patients with bicuspid aortic valve disease and in healthy volunteers. Our findings are in line with the physiological changes during the cardiac cycle and are supported by

validated methodologies, including physiological values of wave speed, supporting the feasibility of the approach. Provided testing in larger cohorts, future research could employ our proposed methodology in order to assess clinical implementation.

Author Contributions: F.S., M.C., C.B.-D. and G.B. were involved in the study design; F.S. and E.D.G. were involved in the data acquisition; E.D.G. and C.B.-D. were involved in gaining ethical approval; F.S., K.D., M.C.K.H. and G.B. were involved in the data analysis; K.D. and G.B. were involved in drafting the manuscript. All authors contributed to the manuscript review. All authors have read and agreed to the published version of the manuscript.

Funding: The authors gratefully acknowledge support from the British Heart Foundation (CH/17/1/32804, AA/18/1/34219), Bristol & Weston Hospitals Charity, and the Bristol NIHR Biomedical Research Centre.

Institutional Review Board Statement: Imaging acquisition received Health Research Authority approval after being reviewed by the Research Ethics Committee (REC) (REC reference: 17/NI/0147).

Informed Consent Statement: Patients and volunteers provided informed consent at the time of MRI scan.

Data Availability Statement: Data requests to be addressed to the corresponding author.

Conflicts of Interest: Chiara Bucciarelli-Ducci is the Chief Executive Officer (part-time) for the Society for Cardiovascular Magnetic Resonance; speaker's fees from Circle Cardiovascular Imaging, Siemens Healthier and Bayer.

References

- van der Linde, D.; Konings, E.E.M.; Slager, M.A.; Witsenburg, M.; Helbing, W.A.; Takkenberg, J.J.M.; Roos-Hesselink, J.W. Birth prevalence of congenital heart disease worldwide: A systematic review and meta-analysis. *J. Am. Coll. Cardiol.* **2011**, *58*, 2241–2247. [[CrossRef](#)] [[PubMed](#)]
- Hope, M.D.; Hope, T.A.; Meadows, A.K.; Ordovas, K.G.; Urbania, T.H.; Alley, M.T.; Higgins, C.B. Bicuspid aortic valve: Four-dimensional MR evaluation of ascending aortic systolic flow patterns. *Radiology* **2010**, *255*, 53–61. [[CrossRef](#)] [[PubMed](#)]
- Atkins, S.K.; Sucosky, P. Etiology of bicuspid aortic valve disease: Focus on hemodynamics. *World J. Cardiol.* **2014**, *6*, 1227–1233. [[CrossRef](#)]
- Lawley, C.M.; Broadhouse, K.M.; Callaghan, F.M.; Winlaw, D.S.; Figtree, G.A.; Grieve, S.M. 4D flow magnetic resonance imaging: Role in pediatric congenital heart disease. *Asian Cardiovasc. Thorac. Ann.* **2017**, *26*, 28–37. [[CrossRef](#)]
- Prakash, A.; Powell, A.J.; Geva, T. Multimodality noninvasive imaging for assessment of congenital heart disease. *Circ. Cardiovasc. Imaging* **2010**, *3*, 112–125. [[CrossRef](#)]
- Mooij, C.F.; de Wit, C.J.; Graham, D.A.; Powell, A.J.; Geva, T. Reproducibility of MRI measurements of right ventricular size and function in patients with normal and dilated ventricles. *J. Magn. Reson. Imaging* **2008**, *28*, 67–73. [[CrossRef](#)] [[PubMed](#)]
- Nayak, K.S.; Nielsen, J.-F.; Bernstein, M.A.; Markl, M.; Gatehouse, P.D.; Botnar, R.M.; Saloner, D.; Lorenz, C.; Wen, H.; Hu, B.S.; et al. Cardiovascular magnetic resonance phase contrast imaging. *J. Cardiovasc. Magn. Reson.* **2015**, *17*, 71. [[CrossRef](#)]
- Chowdhary, A.; Garg, P.; Das, A.; Nazir, M.S.; Plein, S. Cardiovascular magnetic resonance imaging: Emerging techniques and applications. *Heart* **2021**, *107*, 697–704. [[CrossRef](#)]
- Rizk, J. 4D flow MRI applications in congenital heart disease. *Eur. Radiol.* **2021**, *31*, 1160–1174. [[CrossRef](#)]
- Dyverfeldt, P.; Bissell, M.; Barker, A.J.; Bolger, A.F.; Carlhäll, C.-J.; Ebbers, T.; Francios, C.J.; Frydrychowicz, A.; Geiger, J.; Giese, D.; et al. 4D flow cardiovascular magnetic resonance consensus statement. *J. Cardiovasc. Magn. Reson.* **2015**, *17*, 72. [[CrossRef](#)]
- Oyama-Manabe, N.; Aikawa, T.; Tsuneta, S.; Manabe, O. Clinical Applications of 4D Flow MR Imaging in Aortic Valvular and Congenital Heart Disease. *Magn. Reson. Med. Sci.* **2022**, *21*, 319–326. [[CrossRef](#)] [[PubMed](#)]
- Gabbour, M.; Schnell, S.; Jarvis, K.; Robinson, J.D.; Markl, M.; Rigsby, C.K. 4-D flow magnetic resonance imaging: Blood flow quantification compared to 2-D phase-contrast magnetic resonance imaging and Doppler echocardiography. *Pediatr. Radiol.* **2015**, *45*, 804–813. [[CrossRef](#)] [[PubMed](#)]
- Nordmeyer, S.; Riesenkampff, E.; Crelier, G.; Khasheei, A.; Schnackenburg, B.; Berger, F.; Kuehne, T. Flow-sensitive four-dimensional cine magnetic resonance imaging for offline blood flow quantification in multiple vessels: A validation study. *J. Magn. Reson. Imaging* **2010**, *32*, 677–683. [[CrossRef](#)] [[PubMed](#)]
- Hsiao, A.; Tariq, U.; Alley, M.T.; Lustig, M.; Vasanaawala, S.S. Inlet and outlet valve flow and regurgitant volume may be directly and reliably quantified with accelerated, volumetric phase-contrast MRI. *J. Magn. Reson. Imaging* **2015**, *41*, 376–385. [[CrossRef](#)]
- van der Hulst, A.E.; Westenberg, J.J.M.; Kroft, L.J.M.; Bax, J.J.; Blom, N.A.; de Roos, A.; Roest, A.A.W. Tetralogy of fallot: 3D velocity-encoded MR imaging for evaluation of right ventricular valve flow and diastolic function in patients after correction. *Radiology* **2010**, *256*, 724–734. [[CrossRef](#)]

16. Jarvis, K.; Vonder, M.; Barker, A.J.; Schnell, S.; Rose, M.; Carr, J.; Robinson, J.D.; Markl, M.; Rigsby, C.K. Hemodynamic evaluation in patients with transposition of the great arteries after the arterial switch operation: 4D flow and 2D phase contrast cardiovascular magnetic resonance compared with Doppler echocardiography. *J. Cardiovasc. Magn. Reson.* **2016**, *18*, 59. [[CrossRef](#)]
17. van Wijk, W.H.S.; Breur, J.M.P.J.; Westenberg, J.J.M.; Driessen, M.M.P.; Meijboom, F.J.; Driesen, B.; de Baat, E.C.; Doevendans, P.A.F.M.; Leiner, T.; Grotenhuis, H.B. Validation of aortic valve 4D flow analysis and myocardial deformation by cardiovascular magnetic resonance in patients after the arterial switch operation. *J. Cardiovasc. Magn. Reson.* **2019**, *21*, 20. [[CrossRef](#)]
18. She, H.L.; Roest, A.A.; Calkoen, E.E.; van den Boogaard, P.J.; van der Geest, R.J.; Hazekamp, M.G.; de Roos, A.; Westenberg, J.J. Comparative Evaluation of Flow Quantification across the Atrioventricular Valve in Patients with Functional Univentricular Heart after Fontan's Surgery and Healthy Controls: Measurement by 4D Flow Magnetic Resonance Imaging and Streamline Visualization. *Congenit. Heart Dis.* **2017**, *12*, 40–48. [[CrossRef](#)]
19. Rose, M.J.; Jarvis, K.; Chowdhary, V.; Barker, A.J.; Allen, B.D.; Robinson, J.D.; Markl, M.; Rigsby, C.K.; Schnell, S. Efficient method for volumetric assessment of peak blood flow velocity using 4D flow MRI. *J. Magn. Reson. Imaging* **2016**, *44*, 1673–1682. [[CrossRef](#)]
20. Parker, K.H.; Jones, C.J.; Dawson, J.R.; Gibson, D.G. What stops the flow of blood from the heart? *Heart Vessels* **1988**, *4*, 241–245. [[CrossRef](#)]
21. Parker, K.H. An introduction to wave intensity analysis. *Med. Biol. Eng. Comput.* **2009**, *47*, 175–188. [[CrossRef](#)] [[PubMed](#)]
22. Biglino, G.; Steeden, J.A.; Baker, C.; Schievano, S.; Taylor, A.M.; Parker, K.H.; Muthurangu, V. A non-invasive clinical application of wave intensity analysis based on ultrahigh temporal resolution phase-contrast cardiovascular magnetic resonance. *J. Cardiovasc. Magn. Reson. Off. J. Soc. Cardiovasc. Magn. Reson.* **2012**, *14*, 57. [[CrossRef](#)] [[PubMed](#)]
23. Fraser, S.D.; Blakeman, T. Chronic kidney disease: Identification and management in primary care. *Pragmatic Obs. Res.* **2016**, *7*, 21–32. [[CrossRef](#)] [[PubMed](#)]
24. Das, A.; Kelly, C.; Ben-Arzi, H.; van der Geest, R.J.; Plein, S.; Dall'Armellina, E. Acute intra-cavity 4D flow cardiovascular magnetic resonance predicts long-term adverse remodelling following ST-elevation myocardial infarction. *J. Cardiovasc. Magn. Reson. Off. J. Soc. Cardiovasc. Magn. Reson.* **2022**, *24*, 64. [[CrossRef](#)]
25. Zhang, G.; Zhang, S.; Qin, Y.; Fang, J.; Tang, X.; Li, L.; Zhou, Y.; Wu, D.; Yan, S.; Liu, W.V.; et al. Differences in Wall Shear Stress Between High-Risk and Low-Risk Plaques in Patients with Moderate Carotid Artery Stenosis: A 4D Flow MRI Study. *Front. Neurosci.* **2021**, *15*, 678358. [[CrossRef](#)]
26. Gupta, A.N.; Avery, R.; Soulat, G.; Allen, B.D.; Collins, J.D.; Choudhury, L.; Bonow, R.O.; Carr, J.; Markl, M.; Elbaz, M.S.M. Direct mitral regurgitation quantification in hypertrophic cardiomyopathy using 4D flow CMR jet tracking: Evaluation in comparison to conventional CMR. *J. Cardiovasc. Magn. Reson.* **2021**, *23*, 138. [[CrossRef](#)]
27. Hudani, A.; Ihsan Ali, S.; Patton, D.; Myers, K.A.; Fine, N.M.; White, J.A.; Greenway, S.; Garcia, J. 4D-Flow MRI Characterization of Pulmonary Flow in Repaired Tetralogy of Fallot. *Appl. Sci.* **2023**, *13*, 2810. [[CrossRef](#)]
28. Khir, A.W.; O'Brien, A.; Gibbs, J.S.; Parker, K.H. Determination of wave speed and wave separation in the arteries. *J. Biomech.* **2001**, *34*, 1145–1155. [[CrossRef](#)]
29. Li, Y.; Borlotti, A.; Parker, K.H.; Khir, A.W. Variation of wave speed determined by the PU-loop with proximity to a reflection site. In Proceedings of the 2011 Annual International Conference of the IEEE Engineering in Medicine and Biology Society, Boston, MA, USA, 30 August–3 September 2011; IEEE: New York, NY, USA, 2011; pp. 199–202.
30. Rahman, O.; Scott, M.; Bollache, E.; Suwa, K.; Collins, J.; Carr, J.; Fedak, P.; McCarthy, P.; Malaisrie, C.; Barker, A.J.; et al. Interval changes in aortic peak velocity and wall shear stress in patients with bicuspid aortic valve disease. *Int. J. Cardiovasc. Imaging* **2019**, *35*, 1925–1934. [[CrossRef](#)]
31. Mathieu, P.; Bossé, Y.; Huggins, G.S.; Della Corte, A.; Pibarot, P.; Michelena, H.I.; Limongelli, G.; Boulanger, M.C.; Evangelista, A.; Bédard, E.; et al. The pathology and pathobiology of bicuspid aortic valve: State of the art and novel research perspectives. *J. Pathol. Clin. Res.* **2015**, *1*, 195–206. [[CrossRef](#)]
32. Garcia, J.; Beckie, K.; Hassanabad, A.F.; Sojoudi, A.; White, J.A. Aortic and mitral flow quantification using dynamic valve tracking and machine learning: Prospective study assessing static and dynamic plane repeatability, variability and agreement. *JRSM Cardiovasc. Dis.* **2018**, *10*, 2048004021999900. [[CrossRef](#)]
33. Bissell, M.M.; Hess, A.T.; Biasioli, L.; Glaze, S.J.; Loudon, M.; Pitcher, A.; Davis, A.; Prendergast, B.; Markl, M.; Barker, A.J.; et al. Aortic dilation in bicuspid aortic valve disease: Flow pattern is a major contributor and differs with valve fusion type. *Circ. Cardiovasc. Imaging* **2013**, *6*, 499–507. [[CrossRef](#)]
34. Ohyama, Y.; Ambale-Venkatesh, B.; Noda, C.; Kim, J.Y.; Tanami, Y.; Teixido-Tura, G.; Chugh, A.R.; Redheuil, A.; Liu, C.Y.; Wu, C.O.; et al. Aortic Arch Pulse Wave Velocity Assessed by Magnetic Resonance Imaging as a Predictor of Incident Cardiovascular Events: The MESA (Multi-Ethnic Study of Atherosclerosis). *Hypertension* **2017**, *70*, 524–530. [[CrossRef](#)]
35. Devos, D.G.; Rietzschel, E.; Heyse, C.; Vandemaele, P.; Van Bortel, L.; Babin, D.; Segers, P.; Westenberg, J.M.; Achten, R. MR pulse wave velocity increases with age faster in the thoracic aorta than in the abdominal aorta. *J. Magn. Reson. Imaging* **2015**, *41*, 765–772. [[CrossRef](#)]
36. Voges, I.; Jerosch-Herold, M.; Hedderich, J.; Pardun, E.; Hart, C.; Gabbert, D.D.; Hansen, J.H.; Petko, C.; Kramer, H.H.; Rickers, C. Normal values of aortic dimensions, distensibility, and pulse wave velocity in children and young adults: A cross-sectional study. *J. Cardiovasc. Magn. Reson.* **2012**, *14*, 77. [[CrossRef](#)]

37. Milano, E.G.; Neumann, S.; Sophocleous, F.; Pontecorvoli, G.; Curtis, S.L.; Bedair, R.; Caputo, M.; Luciani, G.B.; Bucciarelli-Ducci, C.; Biglino, G. Wave Reflection and Ventriculo-Arterial Coupling in Bicuspid Aortic Valve Patients with Repaired Aortic Coarctation. *Front. Pediatr.* **2021**, *9*, 770754. [[CrossRef](#)]
38. Nistri, S.; Grande-Allen, J.; Noale, M.; Basso, C.; Siviero, P.; Maggi, S.; Crepaldi, G.; Thiene, G. Aortic elasticity and size in bicuspid aortic valve syndrome. *Eur. Heart J.* **2008**, *29*, 472–479. [[CrossRef](#)]
39. Schaefer, B.M.; Lewin, M.B.; Stout, K.K.; Byers, P.H.; Otto, C.M. Usefulness of bicuspid aortic valve phenotype to predict elastic properties of the ascending aorta. *Am. J. Cardiol.* **2007**, *99*, 686–690. [[CrossRef](#)]
40. Johnson, E.M.I.; Scott, M.B.; Jarvis, K.; Allen, B.; Carr, J.; Malaisrie, S.C.; McCarthy, P.; Mehta, C.; Fedak, P.W.M.; Barker, A.J.; et al. Global Aortic Pulse Wave Velocity is Unchanged in Bicuspid Aortopathy with Normal Valve Function but Elevated in Patients with Aortic Valve Stenosis: Insights From a 4D Flow MRI Study of 597 Subjects. *J. Magn. Reson. Imaging* **2022**, *57*, 126–136. [[CrossRef](#)]
41. Singh, A.; Horsfield, M.A.; Bekele, S.; Greenwood, J.P.; Dawson, D.K.; Berry, C.; Hogrefe, K.; Kelly, D.J.; Houston, J.G.; Guntur Ramkumar, P.; et al. Aortic stiffness in aortic stenosis assessed by cardiovascular MRI: A comparison between bicuspid and tricuspid valves. *Eur. Radiol.* **2019**, *29*, 2340–2349. [[CrossRef](#)]
42. Yap, S.-C.; Nemes, A.; Meijboom, F.J.; Galema, T.W.; Geleijnse, M.L.; ten Cate, F.J.; Simoons, M.L.; Roos-Hesselink, J.W. Abnormal aortic elastic properties in adults with congenital valvular aortic stenosis. *Int. J. Cardiol.* **2008**, *128*, 336–341. [[CrossRef](#)] [[PubMed](#)]
43. Grotenhuis, H.B.; Ottenkamp, J.; Westenberg, J.J.M.; Bax, J.J.; Kroft, L.J.M.; de Roos, A. Reduced aortic elasticity and dilatation are associated with aortic regurgitation and left ventricular hypertrophy in nonstenotic bicuspid aortic valve patients. *J. Am. Coll. Cardiol.* **2007**, *49*, 1660–1665. [[CrossRef](#)] [[PubMed](#)]
44. Sophocleous, F.; Biffi, B.; Milano, E.G.; Bruse, J.; Caputo, M.; Rajakaruna, C.; Schievano, S.; Emanuelli, C.; Bucciarelli-Ducci, C.; Biglino, G. Aortic morphological variability in patients with bicuspid aortic valve and aortic coarctation. *Eur. J. Cardio-Thorac. Surg.* **2019**, *55*, 704–713. [[CrossRef](#)]
45. Paraskevas, K.I.; Bessias, N.; Psathas, C.; Akridas, K.; Dragios, T.; Nikitas, G.; Andrikopoulos, V.; Mikhailidis, D.P.; Kyriakides, Z.S. Evaluation of aortic stiffness (aortic pulse-wave velocity) before and after elective abdominal aortic aneurysm repair procedures: A pilot study. *Open Cardiovasc. Med. J.* **2009**, *3*, 173–175. [[CrossRef](#)]
46. Iwahashi, T.; Obitsu, Y.; Koizumi, N.; Shiraishi, Y.; Shigematsu, H. Clinical comparison of two different types of bifurcated graft for postoperative baPWV and ABI. *Int. Angiol.* **2009**, *28*, 232–237.
47. Damughatla, A.R.; Raterman, B.; Sharkey-Toppen, T.; Jin, N.; Simonetti, O.P.; White, R.D.; Kolipaka, A. Quantification of aortic stiffness using MR elastography and its comparison to MRI-based pulse wave velocity. *J. Magn. Reson. Imaging* **2015**, *41*, 44–51. [[CrossRef](#)]
48. Rogers, W.J.; Hu, Y.L.; Coast, D.; Vido, D.A.; Kramer, C.M.; Pyeritz, R.E.; Reichel, N. Age-associated changes in regional aortic pulse wave velocity. *J. Am. Coll. Cardiol.* **2001**, *38*, 1123–1129. [[CrossRef](#)]
49. Taviani, V.; Hickson, S.S.; Hardy, C.J.; McEniery, C.M.; Patterson, A.J.; Gillard, J.H.; Wilkinson, I.B.; Graves, M.J. Age-related changes of regional pulse wave velocity in the descending aorta using Fourier velocity encoded M-mode. *Magn. Reson. Med.* **2011**, *65*, 261–268. [[CrossRef](#)]
50. Alvarez, A.; Martinez, V.; Pizarro, G.; Recio, M.; Cabrera, J.Á. Clinical use of 4D flow MRI for quantification of aortic regurgitation. *Open Heart* **2020**, *7*, e001158. [[CrossRef](#)]
51. Demirkiran, A.; van Ooij, P.; Westenberg, J.J.M.; Hofman, M.B.M.; van Assen, H.C.; Schoonmade, L.J.; Asim, U.; Blanken, C.P.S.; Nederveen, A.J.; van Rossum, A.C.; et al. Clinical intra-cardiac 4D flow CMR: Acquisition, analysis, and clinical applications. *Eur. Heart J. Cardiovasc. Imaging* **2022**, *23*, 154–165. [[CrossRef](#)]
52. Ntsinjana, H.N.; Chung, R.; Ciliberti, P.; Muthurangu, V.; Schievano, S.; Marek, J.; Parker, K.H.; Taylor, A.M.; Biglino, G. Utility of Cardiovascular Magnetic Resonance-Derived Wave Intensity Analysis as a Marker of Ventricular Function in Children with Heart Failure and Normal Ejection Fraction. *Front. Pediatr.* **2017**, *5*, 65. [[CrossRef](#)]
53. Du, G.Q.; Li, H.R.; Xue, J.Y.; Chen, S.; Du, P.; Wu, Y.; Tian, J.W. Wave Intensity Analysis Can Identify Eccentric Cardiac Hypertrophy in Hypertensive Patients with Varied Left Ventricular Configurations. *J. Ultrasound Med.* **2015**, *34*, 2019–2027. [[CrossRef](#)]
54. Broyd, C.J.; Davies, J.E.; Escaned, J.E.; Hughes, A.; Parker, K. Wave intensity analysis and its application to the coronary circulation. *Glob. Cardiol. Sci. Pract.* **2017**, *2017*, e201705. [[CrossRef](#)]
55. Wang, J.; Deng, W.; Lv, Q.; Li, Y.; Liu, T.; Xie, M. Aortic Dilatation in Patients with Bicuspid Aortic Valve. *Front. Physiol.* **2021**, *12*, 615175. [[CrossRef](#)]
56. Corrado, P.A.; Seiter, D.P.; Wieben, O. Automatic measurement plane placement for 4D Flow MRI of the great vessels using deep learning. *Int. J. Comput. Assist. Radiol. Surg.* **2022**, *17*, 199–210. [[CrossRef](#)]

Disclaimer/Publisher's Note: The statements, opinions and data contained in all publications are solely those of the individual author(s) and contributor(s) and not of MDPI and/or the editor(s). MDPI and/or the editor(s) disclaim responsibility for any injury to people or property resulting from any ideas, methods, instructions or products referred to in the content.